Pergamon

Journal of Structural Geology, Vol. 18, No. 12, pp. 1471 to 1486, 1996

PII: S0191-8141(96)00059-4
0191-8141/96 $15.00+0.00

Transient discontinuities revisited: pseudotachylyte, plastic instability and the influence of low pore fluid pressure on deformation processes in the mid-crust

JOSEPH CLANCY WHITE*

Department of Geology, The University of New Brunswick, Fredericton NB, Canada E3B 5A3

(*Received* 17 *July* 1995; *accepted in revised form* 27 *June* 1996)

Abstract—Occurrences of pseudotachylyte cyclically introduced as melts into the Outer Hebrides thrust are demonstrably synkinematic with crystal–plastic mylonites. Classical interpretations of these rock types as, respectively, products of pressure-dependent frictional melting and thermally-activated intracrystalline deformation create a paradox in that these processes are, to a large extent, mutually exclusive. Detailed microstructural and microcompositional analyses of host mylonites and primary and deformed pseudotachylyte were carried out by light and electron microscopy. The ambient shear zone environment in which pseudotachylyte formed was determined to comprise temperatures in the order of 500° C and stresses of 140–210 MPa, on which were imposed much higher transient stresses in response to heterogeneous, non-uniform flow. The latter conditions are sufficient for the development of plastic instabilities in feldspar-rich crust, if pore fluid pressures are sufficiently low. The latter is consistent with the absence of hydration during exhumation observed in the rocks under study. Low pore fluid pressure during thrust exhumation of deep crust enables activation of high-strength ductile processes dominated by dislocation glide which may be a prerequisite to instability. Whereas other studies have demonstrated the possible occurrence of such melt-generating instabilities, it is believed that this study provides the first example in which the calculated potential for instability formation is consistent with the deformation microstructures and estimated pressure–temperature conditions. Grain-size reduction to produce ultramylonites dominated by grain-size-sensitive flow is achieved by both deformation-induced dynamic recrystallization and crystallization of instability-generated melts. Copyright © 1996 Published by Elsevier Science Ltd

INTRODUCTION

The resolution of the recurring debate over conditions under which ductile shear flow can produce thermal perturbations that lead to melting (Nicolas *et al.* 1977, Brun & Cobbold 1980, Fleitout & Froidvaux 1980, Scholz 1980, Hobbs *et al.* 1986, Pavlis 1986, Frischbutter & Hanisch 1991) ultimately requires testing in the geologic record. Coeval occurrences of pseudotachylyte and mylonite (Seaforth Head, Outer Hebrides thrust, Sibson 1980a; Saint-Barthelemy Massif, French Pyrenees, Passchier 1982; Redbank shear zone, central Australia, Hobbs *et al.* 1986; Silvretta nappe, Eastern Alps, Koch & Masch 1992) are particularly relevant to this controversy. Pseudotachylyte generated by frictional, stick-slip melting (McKenzie & Brune 1972, Sibson 1975, Spray 1987) is well established as a product of fault zone deformation that develops in response to high differential stress. However, a paradox exists in the synchronous development of pseudotachylyte with mylonite in that their presumed mechanisms of formation are competitive, and to a significant degree, mutually exclusive. Whereas frictional melting is typically associated with pressure-dependent, spatially-localized velocity-weakening behaviour, mylonitization is characterized by grain-scale plasticity and diffusion during more distributed, thermally-activated aseismic flow (Sibson 1977).

Deformation paths suggested to resolve this paradox include:

(A) cyclic generation of pseudotachylyte within deforming mylonites as a thrust block moves through the base of the seismogenic zone, i.e. a normal exhumation overprinting sequence at the brittle–ductile transition (Passchier 1982, Koch & Masch 1992) consistent with peak strength behaviour at the base of the seismogenic zone (Sibson 1977, Brace & Kohlstedt 1980);

(B) brittle failure within the ductile regime (Sibson 1980a) below the general seismogenic zone resulting from: (i) dynamic fracture propagation downward from the seismogenic zone, (ii) fracture initiation at stress concentrations produced by rheologically-contrasting inclusions or (iii) an effective increase in the ambient geothermal gradient by shear heating which would decrease the depth at which thermally-activated processes are significant, thus introducing ductile deformation into a shallower crustal level at which frictional strengths are in turn lower due to the reduction in mean stress;

(C) development of plastic instabilities in the ductile regime that produce temperature transients leading to melting (Sibson 1980a, Hobbs *et al.* 1986).

Each path constrains the conditions of pseudotachylyte formation. Path A limits ambient fault/shear zone temperatures to less than 300°–400° C (Sibson 1984), even for relatively steep geothermal gradients. Path B is limited by the distance over which melt-initiating fractures can propagate or the degree of stress concentration that can be generated during ductile flow. The conditions for which Path C is relevant are defined by a limiting critical upper temperature, for a given rheology, above which thermo–mechanical instabilities are precluded (Hobbs *et al.* 1986, Ord & Hobbs 1989).

Previous studies of mylonite–pseudotachylyte assemblages (Passchier 1982, Hobbs *et al.* 1986, Koch & Masch 1992), although extolling different processes, tend to place formation of the pseudotachylyte at greenschist

*Fax: 506 453 5055. E-mail: clancy@unb.ca

grade temperatures (300–400°C), or lower, that correspond to depths of less than 12–15 km. The latter conditions are within the recognized seismogenic zone for which models of continental fault architecture (Sibson 1977) predict high-strength behaviour compatible with frictional melting. Nevertheless, consideration of thermo-mechanical regimes in the lithosphere (Ord & Hobbs 1989) suggests that stresses sufficient to induce ductile instability could exist throughout much of the crust. In support of this proposition, field and thin-section observations on the Seaforth Head segment (Sibson 1980a) of the Outer Hebrides thrust (OHT) infer amphibolite-grade deformation, suggesting pseudotachylyte formation at approximately 500° C and depths of 17–25 km, depending on the chosen geothermal gradient. At such depths, pressure-dependent, dry frictional slip (Byerlee 1978, Sibson 1974, Scholz 1990) requires extreme differential stress in excess of 1 GPa, an order of magnitude greater than most estimates of either seismic or aseismic stresses (Hanks 1977, Hanks & Raleigh 1980, Mercier 1980, Etheridge 1983, Sibson 1986, Engelder 1993 and refs therein).

The question at the core of this study remains, to what crustal depth can pseudotachylyte form and by what mechanism(s) is it achieved? This question is particularly seminal to the behaviour of crustal shear zones and the distribution of mechanical processes given reports of pseudotachylyte forming at depths well outside the 'normal' seismogenic zone (Clarke & Norman 1993, Austrheim & Boundy 1994). Likewise, the high energy release anticipated during pseudotachylyte-generating events (Sibson 1980b) has consequences for interpretations of large magnitude earthquakes (Shimamoto 1985) and the development of seismic gaps in megathrust systems. Although the general conditions under which plastic instabilities could develop have been described (Hobbs *et al.* 1986, Hobbs & Ord 1988), an understanding of the temperature and depth of formation, and ensuing microstructures of specific mylonite-pseudotachylyte occurrences, is necessary in order to test the validity of such processes in natural systems, particularly given their implications for seismic behaviour of the lithosphere.

The mylonite-pseudotachylyte occurrence at Seaforth Head provides an opportunity to scrutinize the details of pseudotachylyte formation in ductile regimes. This occurrence has distinct attributes, in common with others (Hobbs *et al.* 1986) that are relevant to the subsequent discussion. These include: (1) development in a thrust regime, (2) cyclic generation and subsequent ductile deformation of large volume fractions of pseudotachylyte within an otherwise 'normal' shear zone, and (3) a general absence of retrogression and hydration within the host rocks and pseudotachylyte.

METHODOLOGY AND INSTRUMENTATION

Material from the original study area of Sibson (1980a) at Seaforth Head has been re-examined to determine: (i) the nature of primary pseudotachylyte veins; (ii) the microstructural and mineral composition history of the deformed pseudotachylyte veins and (iii) the micromechanisms and associated deformation environment inferred to exist during generation and deformation of the pseudotachylyte. Specifically, the synkinematic microstructure of deformed pseudotachylyte veins is anticipated to carry a record of the deformation environment that reflects only the interval since its injection. Because the pseudotachylyte is cyclically introduced, as demonstrated by cross-cutting relationships during transposition, comparison of the microstructural and compositional records among the host mylonite and deformed pseudotachylytes has the potential to establish variations in rheological behaviour and metamorphic environment with time.

The ultra-fine-grained nature of these types of rock have in the past limited their detailed study. Previous workers have concentrated on thin-section examination (Sibson 1980a, Hobbs *et al.* 1986), although Passchier (1982) also utilized secondary electron imaging by scanning electron microscopy (SEM) and Koch & Masch (1992) examined quartz with transmission electron microscopy (TEM). This study emphasizes combined optical and analytical scanning and transmission electron microscopy. Instrumentation comprised a JEOL 6400 SEM with combined wavelength and LINK eXL energy-dispersive x-ray analytical systems and a Philips EM400T TEM with a LINK Pentafet light-element energy-dispersive detector and eXL x-ray analyzer. The TEM was operated at 120 keV, except for some standardized analyses, which were done at 100 keV.

GEOLOGICAL SETTING

The geological setting of the study area (Fig. 1) has been described in detail by Sibson (1980a). In the Seaforth Head region, amphibolite grade gneisses are variably deformed within the Outer Hebrides thrust (Francis & Sibson 1973) over a 1 km wide, shallowly dipping shear zone with the cyclic introduction and subsequent deformation of pseudotachylyte apparent in the field. Pseudotachylyte can form 50% of the outcrop. The cross-cutting relationships of various generations of pseudotachylyte veins and their progressive transposition into the mylonite fabric is confirmed in thin section. Metamorphic mineral assemblages vary as a function of rock bulk composition, but typically comprise hornblende, plagioclase (An25–An60), orthoclase, biotite, garnet and quartz. As described by Sibson (1980a), there is a notable absence of retrogression and hydration typical of other highly deformed segments of the Outer Hebrides thrust, requiring that this be either a deeper section of the fault zone than exposed elsewhere or fortuitously preserved low permeability material which was not hydrated during exhumation. The absence of retrogression is central to interpretation of the deformation environment and generation of the pseudotachylyte.

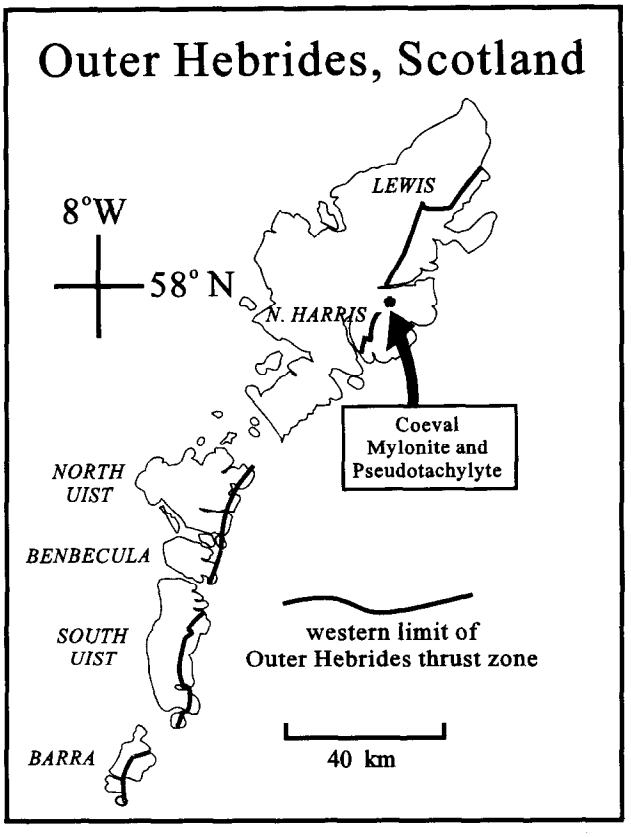

Fig. 1. Location map for study area (star) at Seaforth Head, Isle of Lewis, along the Outer Hebrides thrust.

DEFORMATION MICROSTRUCTURES

Mylonitic gneisses

The mylonitized gneisses exhibit intense strain gradients and variations in microstructural response to the imposed deformation, with extensive non-uniform flow at the grain scale; for example, feldspar porphyroclasts (100 μm diameter) are commonly enveloped by micrometre-thick foliae of recrystallized grains (Fig. 2a; see also fig. 2 of Sibson 1980a). The accumulation of intracrystalline strain, combined with grain-size reduction typifies the overall optical microstructure. Recrystallized grains of plagioclase, K-feldspar and amphibole in the mylonite matrix are typically 1–2 μm in diameter, while quartz ranges between 4–12 μm in diameter. There is minimal optical evidence of recovery substructures developing prior to recrystallization. Large, mm-scale K-feldspar (orthoclase) porphyroclasts exhibit dramatic grain-size reduction that can sometimes be suggestive of cataclasis and flow at high confining pressure (Fig. 2b). However, TEM shows there to be no extensive fracturing, intracrystalline rotation or healed cracks typical of brittle deformation and instead documents recrystallization in response to high dislocation densities (Figs. 2c–e) as observed experimentally in the dislocation creep field (compare with fig. 2 of Tullis & Yund 1987).

The defining attribute of the mylonite is the ubiquity of free dislocations (Fig. 2c) in host grains in which dislocation densities varying from 5×10^{12} m^{-2} in quartz, to in excess of 10^{14} m^{-2} in K-feldspar. Crystallographic fabrics, as indicated by retardation plate colours, are intense, particularly in quartz, attesting to the activity of dislocation glide. Quartz exhibits the highest degree of dislocation interaction and readjustment, although subgrains remain rare. The latter emphasizes the high ratio of glide versus climb in these rocks, relative to that typically seen in quartz-rich mylonites deformed in the dislocation creep regime. Invisibility experiments and trace analysis of K-feldspar dislocations indicate glide on (010)<001>, (010)<101> and (001)<110> slip systems. Despite dislocation densities commonly in excess of 10^{13} m^{-2}, there is a notable absence of dislocation tangles characteristic of cold-working and fracture initiation (Stesky *et al.* 1974, Stesky 1978, White & White 1983, Tullis & Yund 1992), although a very few glide bands defined by zones of concentrated dislocations are observed (Fig. 2d).

Dynamic recrystallization of feldspar porphyroclasts occurs across narrow grain mantles (Gifkins 1976) that are typically one subgrain wide. Subgrains concentrated at grain boundaries comprise the principal microstructural evidence for limited recovery and are transitional between high dislocation densities in the host grain cores and equant, relatively dislocation-free recrystallized grains (Fig. 2e; compare with fig. 2 of Tullis & Yund 1987). The overall absence of dislocations in the recrystallized grains suggests grain-boundary migration as the operative recrystallization process. The abruptness of recrystallization with little evidence of intracrystalline strain contributes to the optical similarity with cataclasis. Al–Si ordering textures (tweed) and albite exsolution lamellae are more fully developed in host grain mantles and in recrystallized grains, pointing to dislocation-enhanced intracrystalline transformations, associated with the recrystallization front, and sufficient temperature for alkali diffusion. The concomitant exsolution of albite with recrystallization produces a 2-phase aggregate of micrometre diameter grains. Flame perthite occurs rarely (Fig. 2b), providing evidence for limited dilation and fluid ingress during deformation (Pryer 1993).

Amphibole textures provide the most persuasive evidence for brittle processes and associated fluids. Sharp dislocation walls parallel to {110} cleavage planes define grain boundaries that are frequently decorated with precipitates and are interpreted as healed fractures. Recrystallized grains have strongly etched grain boundaries that locally contain chlorite. Stacking faults extend in from grain boundaries, presumably in response to cation exchange with metamorphic fluids (Fig. 2f). Quartz grains within the amphibole recrystallization tails commonly contain impurity phases and exhibit much faster ionization damage in the electron beam than other quartz, suggesting a high hydroxyl content, both observations being consistent with fluid-precipitated quartz. Dislocation densities are more variable in amphibole than in the other phases, but average about 6×10^{12} m^{-2}. The limited evidence for fracture and fluid access in the amphibole serves to emphasize the general absence of pervasive fluid-enhanced fracturing in these rocks.

Pseudotachylyte

Primary pseudotachylyte occurs as dykes, veins and dilational blobs that cross-cut the gneissic foliation (see Fig. 1 of Sibson 1980a). In thin section, pseudotachylyte consists of silicate fragments in a black, optically isotropic, unfoliated matrix. Porphyroclasts are predominantly quartz, followed by plagioclase and K-feldspar, while the matrix comprises a submicrometre aggregate of amphibole and plagioclase, with lesser amounts of quartz, K-feldspar and ilmenite (Fig. 3a). There is abundant evidence for the melt origin of the pseudotachylyte. Micro-ophitic crystallization textures between plagioclase and amphibole (Fig. 3b) are common, as is the corrosion of hornblende grains by the matrix at the vein boundaries. Some coarser amphibole aggregates have grain boundaries impregnated with plagioclase, as if wetted by a melt phase. Melt intergrowths of feldspar and quartz occur as clasts (Fig. 3c), while quartz clasts can be surrounded by radiating grains. Aggregate clasts contain evidence of cataclasis in the form of welded dilatant fractures, presumably related to their incorporation into the melt (Fig. 3a), while both clasts and host material can be injected by matrix material (Fig. 3b). TEM shows a generally random array of fine-grained material with sharp, distinct grain contacts. Matrix (melt) grains vary in size from 100 nm–1 μm and are largely dislocation-free (Fig. 3d).

Deformed pseudotachylyte

Colour change distinguishes pseudotachylyte veins in various stages of transposition. Veins of dark, optically isotropic, primary pseudotachylyte progressively alter though shades of brown to a greenish, foliated compositional banding, giving an end product that is an optically isotropic ultramylonite (Fig. 4a; see also Sibson 1980a, Passchier 1982, Hobbs *et al.* 1986) and is intimately mixed with fine-grained material that need not have originated as primary pseudotachylyte. Individual feldspar porphyroclasts exhibit shear fractures containing older pseudotachylyte that is truncated by later pseudotachylyte at the porphyroclast boundary. The optically homogeneous ultramylonite bands exhibit fine-scale compositional layering in back-scattered electron images (BSEI) that reflects modal variations in plagioclase and amphibole. Biotite comparable to that in the host gneiss is found, and only in small modal proportions ($<1\%$), which with very minor chlorite associated with amphibole comprise the only phyllosilicates. There is no evidence for extensive hydration and new phyllosilicate formation.

Extreme shear flow of the deformed pseudotachylyte/ultramylonite is attested to by elongated, rotated and folded porphyroclasts, in addition to folding and transposition of the layers themselves (Figs. 4a & b). Interference folds are common and often have geometries typical of sheath folds. Porphyroclasts are predominantly plagioclase, followed by K-feldspar and amphibole, that range in size from 3 mm to less than 10 μm and comprise a mixture of porphyroclasts from primary pseudotachylyte and host material incorporated during transposition of the veins.

Substructures within porphyroclasts are similar to those observed in the host mylonites. Subgrains are rare and are cut by dislocations (Fig. 4c). Dislocation densities in plagioclase porphyroclasts range from 0.90–1.4×10^{13} m^{-2}, with glide identified on (010)<100> and (010)<101> systems. Recrystallization of the porphyroclasts contributes to the formation of compositional layering. Dynamic recrystallization textures of quartz, plagioclase and K-feldspar porphyroclasts show no definitive evidence of comminution or related brittle processes, whereas amphibole recrystallization textures are more ambiguous. Amphibole tends to recrystallize as micrometer-scale aggregates of plagioclase and amphibole, with the formation of a 2-phase mantle (plagioclase–amphibole) within the host grain a precursor to the recrystallization. The latter suggests metamorphic equilibration of plagioclase and amphibole during recrystallization. This texture strongly resembles cataclastic textures described by Nyman *et al.* (1992), although no comparable systematic change in amphibole composition was identified (see Mineral Composition Effects).

Grains forming the matrix to the porphyroclasts in the deformed pseudotachylyte are derived from both the primary pseudotachylyte and recrystallization of porphyroclasts during deformation as an ultramylonite. Matrix grains are generally equant, but can be moderately elongate parallel to the foliation (Fig. 4d), particularly when a product of recrystallization. Dislocation densities are low and are heterogeneously developed among grains where present. Notably, the most intense macroscopic strains develop where matrix grains show neither shape fabric nor evidence of intracrystalline deformation (see Deformation Mechanisms). Grains with high dislocation densities tend to be derived from and adjacent to recrystallized porphyroclasts, consistent with rotation recrystallization during dislocation creep of the coarse-grained material. Dislocations are most common in quartz, in which dislocation densities are essentially bimodal, i.e. virtually dislocation-free grains or densities of about 6×10^{12} m^{-2}. K-feldspar occurs as strongly modulated orthoclase, sometimes with albite exsolution, but no microcline was observed. Textural re-adjustment of primary pseudotachylyte during deformation includes a general increase in grain size, which ranges from 400 nm to 3 μm in deformed layers, and formation of more curvilinear grain boundaries than in the primary pseudotachylyte (Fig. 4e & f, and compare with Fig. 3b & d).

Brecciation

Late stage brittle discontinuities disrupt the mylonite–ultramylonite foliation, giving a blocky texture. Fractures are clean, and commonly have only micrometre wide disruption zones. Even where there is evidence of dilation, the fracture is filled with the same composition material as the fractured host. These textures suggest minimal pore fluids in response to either an inherently

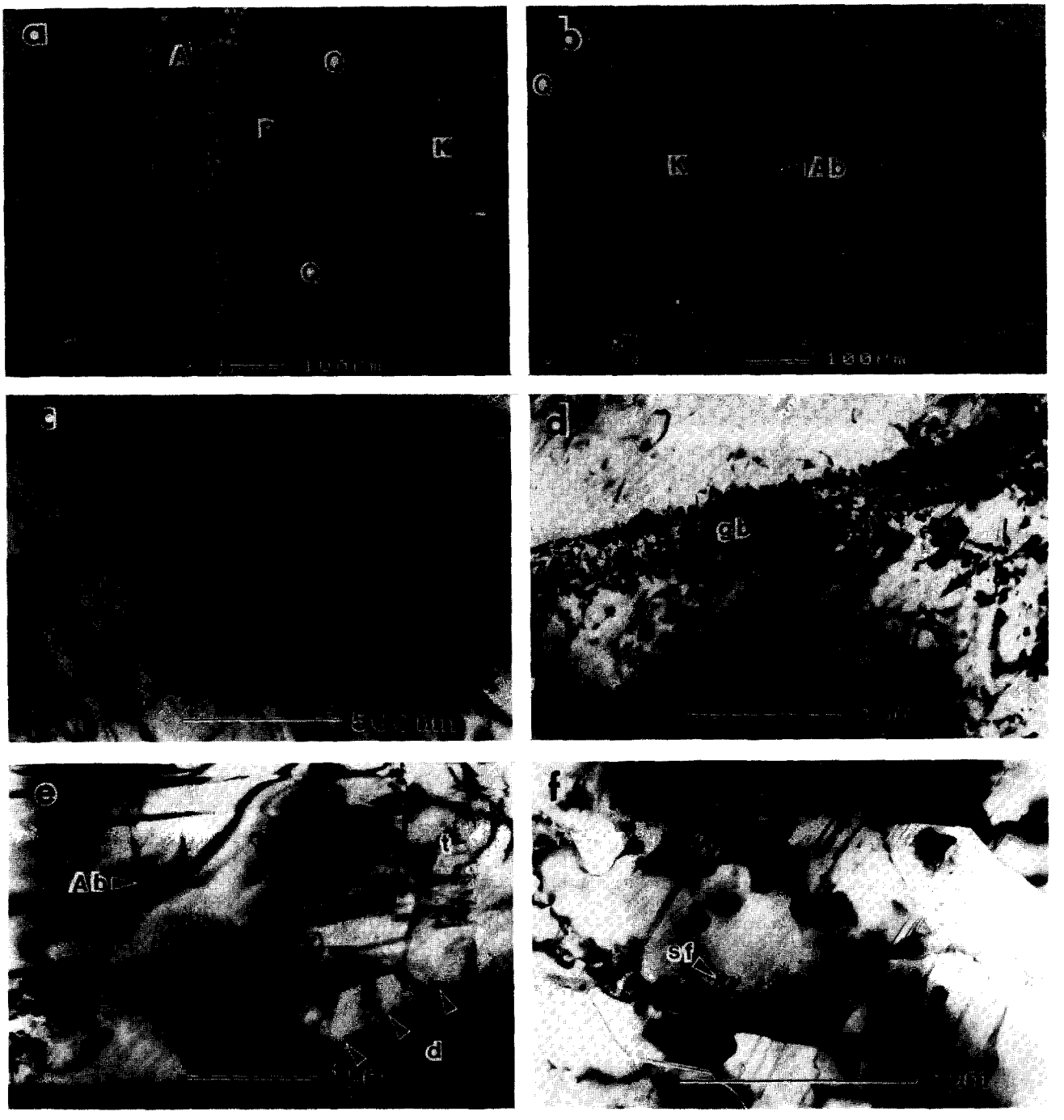

Fig. 2. Mylonitic gneisses. (a) Non-uniform flow textures in mylonitic gneiss that is both the host rock to and forms coevally with pseudotachylyte. Plagioclase (P) and K-feldspar (K) porphyroclasts exhibit intense recrystallization, while quartz (Q) forms elongate ribbons. Amphibole (A) shows minimal grain distortion prior to recrystallizing as equant grains. Back-scattered electron image—BSEI. (b) Recrystallization of K-feldspar porphyroclasts (K), quartz ribbon (Q) and rare occurrence of albite (Ab) as flame perthite, the latter suggesting there is some access to water during deformation, but that it is minimal. BSEI. (c) Dislocation glide on (010) planes in K-feldspar (010). TEM Brightfield image (BF); $g = 002$ (operative diffracting vector). (d) Glide band (gb) defined by zone of concentrated dislocations in a heavily dislocated K-feldspar grain. TEM BF; $g = 002$. (e) Dynamic recrystallization in K-feldspar. Heavily dislocated grains, d, exhibit subgrain development and formation of new, relatively strain-free grains along a narrow host mantle (arrows) typically one subgrain wide. Exsolution of albite (Ab) and formation of tweed texture (t) reflecting Al/Si ordering are concentrated at recrystallization interfaces. TEM BF; $g = 002$. (f) Recrystallized amphibole with grain boundaries parallel to {110} planes suggesting that cleavage fracture may be involved in the grain size reduction process. Stacking faults (sf) propagate in from grain boundaries, possibly initiated by fluid access along the grain boundaries leading to subsequent cation exchange. The evidence for some minimal fluid ingress is used to argue for its general absence during deformation. TEM BF.

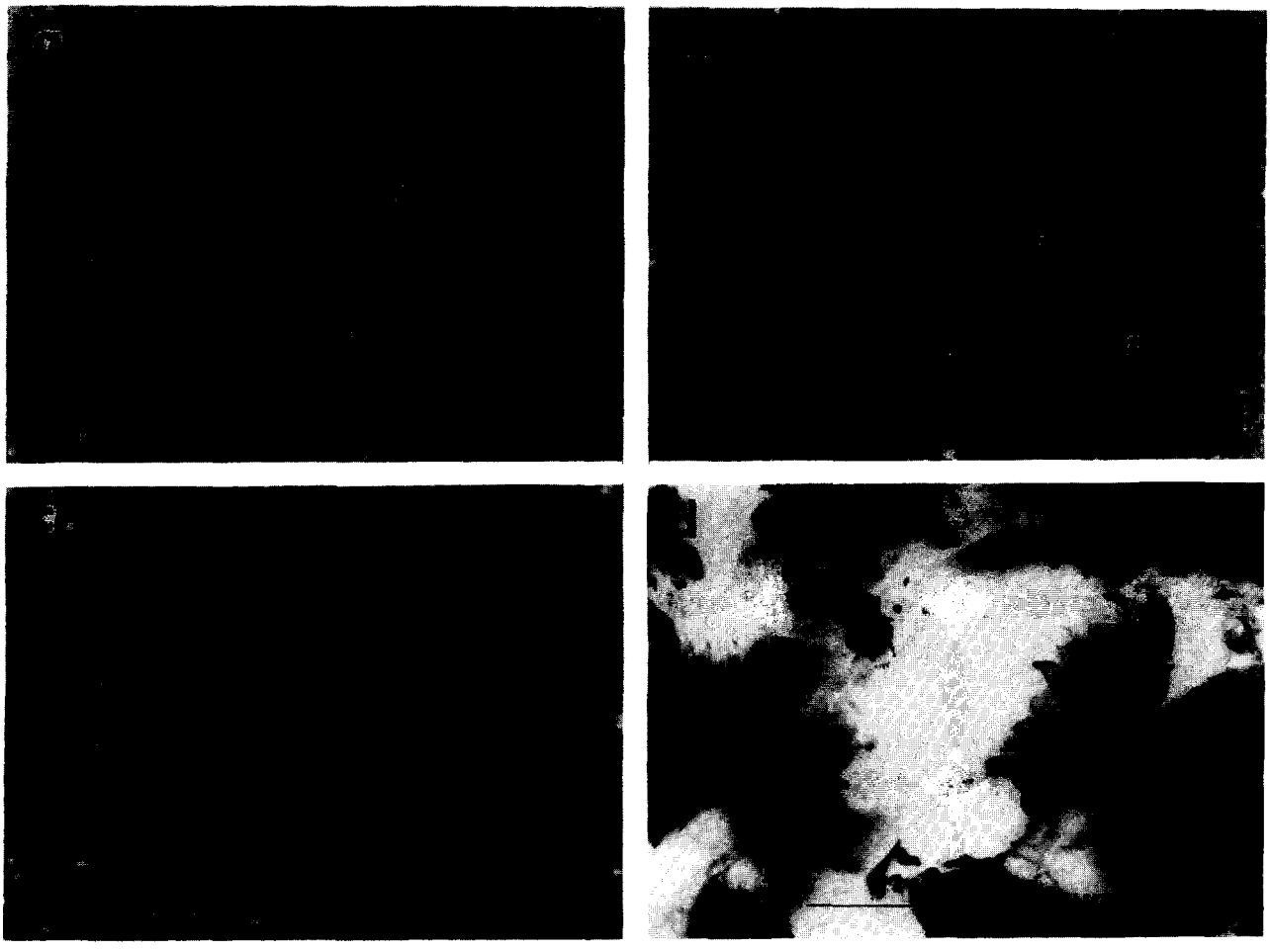

Fig. 3. Pseudotachylyte. (a) Overview of undeformed pseudotachylyte comprising clasts of quartz (Q) and plagioclase (P) in a submicrometre matrix of grains. BSEI. (b) Micro-ophitic texture comprising laths of amphibole (A) and plagioclase (P) indicative of crystallization from a melt. Clasts are primarily quartz (Q). BSEI. (c) K-feldspar (light colour) and quartz (dark) intergrowth (i) formed during crystallization of melt. The matrix comprises very fine-grained amphibole, plagioclase, K-feldspar with some oxides and quartz. BSEI. (d) Pseudotachylyte matrix is a polymineralic aggregate with grain sizes in the range of 100 nm to 1 μm. Grain shapes are equally variable and grain boundaries are irregular. TEM BF.

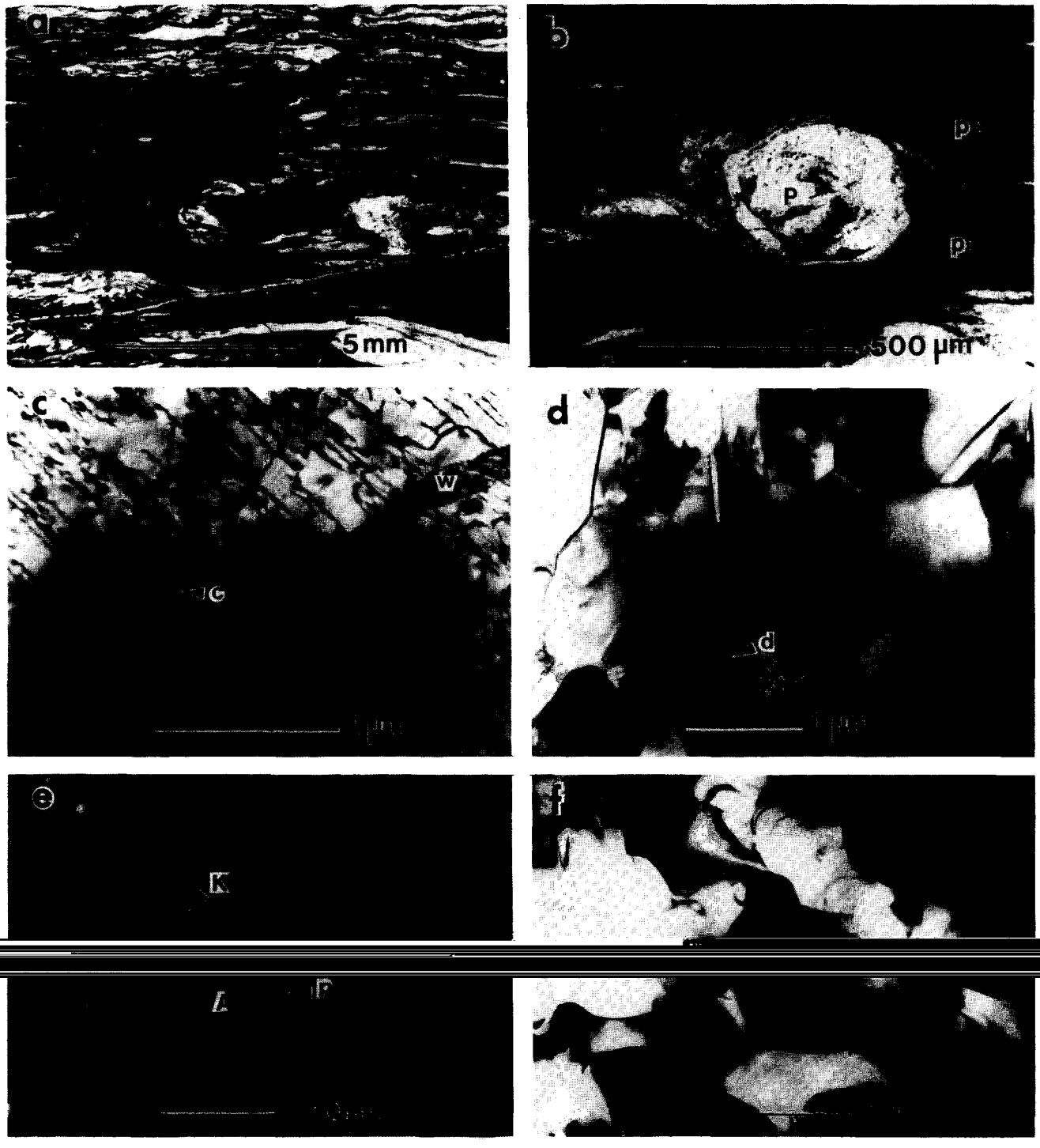

Fig. 4. Ultramylonite (deformed pseudotachylyte). (a) Flow textures in ultramylonite demonstrating heterogeneity of flow, deformed porphyroclasts and transposition of pseudotachylyte in ductile regime. Light microscope, plane polarized light (PPL). (b) Deformed, recrystallized and rotated plagioclase (P) porphyroclast in ultramylonite. Variations in grain size allow differentiation of older (p1) and younger (p2) pseudotachylyte layers. In general, grain size increases during ductile deformation of pseudotachylyte. Light microscope PPL. (c) Dislocations in plagioclase porphyroclast in ultramylonite. Evidence for recovery in the form of subgrain walls (w) is scant, where they occur they are cut by dislocations. Equally uncommon are cracks, c, the general absence of which emphasizes the ductile nature of the deformation. TEM BF. (d) Matrix grains formed by dynamic recrystallization of plagioclase during ultramylonite flow. Grains can be somewhat elongate parallel to the foliation and exhibit some dislocation activity (d), albeit minor. TEM BF. (e) Ultramylonite (deformed pseudotachylyte) texture that is analogous to polyphase superplastic alloys. There has been a distinct increase in grain size and equilibration of grain boundary textures relative to undeformed pseudotachylyte (compare with Fig. 3c). A—amphibole; K—K-feldspar; P—plagioclase BSEI. (f) Equant grains and curvilinear grain boundaries typical of ultramylonite (compare with Fig. 3d). Grains are effectively dislocation free except proximal to recrystallizing porphyroclasts e.g. (d). TEM BF.

low fluid content of the rocks or a low permeability relative to any adjacent crustal reservoir.

MINERAL COMPOSITIONAL EFFECTS

General statement

The deformed pseudotachylyte potentially contains critical compositional evidence of the synkinematic metamorphic conditions that can, in principle, differ from any record inherited by the mylonites from the host gneisses. Standard geothermometry is limited by the existing mineral assemblages and the very fine grain size of the most relevant material. To circumvent these difficulties, trends in plagioclase and amphibole compositions were examined with the expectation that they will indicate any deviation in the deformation environment from the amphibolite grade of the host gneisses. Four indicators of metamorphic temperature were considered: (1) changes in the anorthite component of plagioclase, (2) composition of host and recrystallized amphibole, (3) NaSi $\rightleftharpoons$ CaAl exchange equilibrium between amphibole and plagioclase, and (4) the orthoclase $\rightarrow$ microcline transformation.

Plagioclase compositions

Plagioclase clasts in the primary pseudotachylyte have bimodal compositions (the majority being $\approx$An36 and a few of $\approx$An60) that reflect initial compositions in the host gneisses. Only the lower An-content grains are sufficiently common for systematic analysis. Host and recrystallized grains large enough to be analyzed by SEM range from An23 to An41 (An_{avg} = An31, *s.d.* = 4.5, n = 44). Only one case of systematic compositional variation between host and recrystallized grains was observed, with grain core compositions of An28 becoming increasingly sodic (An18) in the recrystallized tail, consistent with a retrograde trend. Micrometre-scale mylonite and ultramylonite matrix grains were analyzed in TEM with compositions standardized against grains analyzed in the SEM by combined WDS/EDS x-ray analysis. Compositions range from An19–An41 with a mean composition of An29 (*s.d.* = 7.3, n = 33). The standard deviation for TEM analyses is larger, but the results fall within the compositional range determined by SEM microprobe analysis. Although it cannot be statistically discriminated, there is a sense that the average anorthite component is decreasing from host gneisses to mylonite to highly deformed ultramylonite (e.g. An36 $\rightarrow$ An31 $\rightarrow$ An29). This trend is supported by the one case of host-matrix variation, but there remains limited evidence for retrogression during the deformation. If only the statistical variations are considered, plagioclase compositions remain unchanged throughout the pseudotachylyte–mylonite cycle. With or without retrogression, plagioclase composition 'more calcic than An20 (commonly about An30)' is a classical indicator of amphibolite facies (Turner 1968 p.308).

Amphibole compositions

Recrystallized amphiboles in the ultramylonites tend to reflect the initial compositions of host grains (Fig. 5). When core–rim or host–daughter compositions do vary in dynamically recrystallized porphyroclasts (Fig. 6), the increasing (Na + AlIV)/Si is consistent with prograde conditions (Cumbest *et al.* 1989). Given that the rocks are deformed during thrust exhumation, the latter variation can be interpreted as either a relict of pre-pseudotachylyte metamorphism or limited prograde reaction induced by heat within the pseudotachylyte. Overall, as with plagioclase, amphibole compositions suggest formation and deformation of pseudotachylyte at the same conditions at which mylonitization occurred in the host gneisses.

Plagioclase–amphibole equilibrium

The empirical geothermometer of Spear (1980) has been applied to the Seaforth Head rocks, while remaining cognizant of the uncertainties in formulae calculations and bulk rock composition that could induce error. The range of Ca(M4)/Na(M4) ratios (8.2–22.2) determined from calculated formula units, in conjunction with the complete range of plagioclase compositions (An18–An41) constrains temperatures between 480–600° C. Incorporating the 50° C uncertainty in the model (Spear 1980) gives a minimum temperature estimate of 430° C. The best constrained analyses of co-existing amphibole and plagioclase grains, typically a modally significant composition of about An29, give a more limited range of 510–530° C, or a minimum of 460° C when the maximum model error is incorporated. Notably, the latter estimates are consistent with the amphibolite facies classification obtained using classical mineral assemblages (Robinson *et al.* 1982).

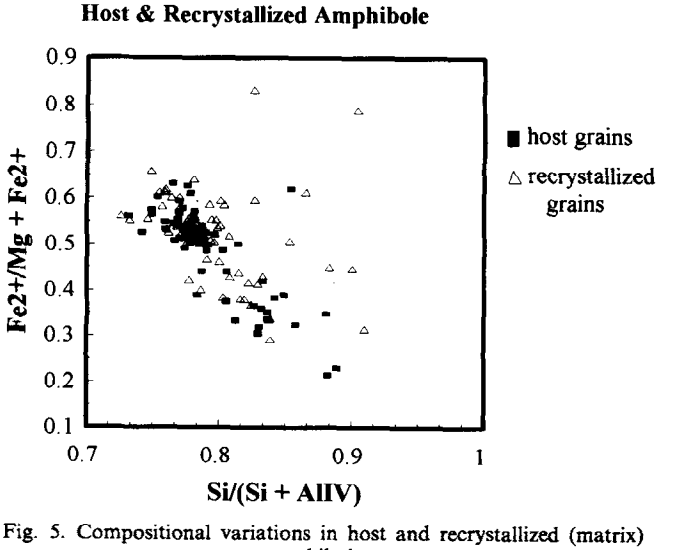

Fig. 5. Compositional variations in host and recrystallized (matrix) amphiboles.

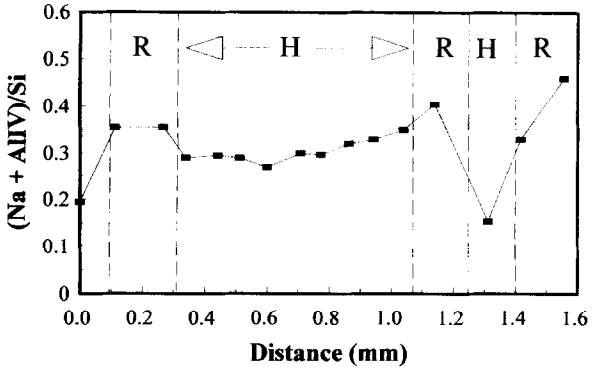

Fig. 6. Most extreme compositional variations found across a single amphibole grain. H—host; R—recrystallized grains.

Orthoclase → microcline transformation

Although K-feldspar occurs as both orthoclase (monoclinic) and microcline (triclinic), orthoclase is much more common, forming all of the pseudotachylyte and ultramylonite matrix grains, the large porphyroclasts and the majority of recrystallized grains. When microcline is observed, it is restricted to the dislocation-rich edge of dynamically recrystallizing porphyroclasts and recrystallization tails. During cooling of metamorphic orthoclase, Al/Si ordering in tetrahedral sites produces the characteristic tweed modulation seen in TEM (Fig. 2e). Brown & Parsons (1989) suggest that the modulation textures varies strongly at temperatures below about 500–525° C and that the monoclinic–triclinic transformation lies above 450° C. However, ambiguity in the interpretation of microstructures associated with this transformation arises from the energetic inhibition of complete ordering that is induced by the tweed modulation and which must be overcome through the aid of dislocation glide or fluid-enhanced diffusion if microcline is to develop (see Eggleton & Buseck 1980 and Brown & Parsons 1989 for discussion of this effect). The transformation in this study is intimately linked to high strain zones undergoing dynamic recrystallization, but even in these kinetically favourable sites, grains are not transformed (i.e. not twinned). The 450–525° C range over which textural changes in the K-feldspar are expected, corresponds well to the plagioclase–amphibole temperature estimates.

DISCUSSION

Deformation summary and flow laws

Detailed microstructural analysis has established several key elements of the deformation at Seaforth Head which have hitherto been largely inferred. Within an outwardly 'normal' ductile shear zone, deforming under amphibolite conditions at temperatures in excess of a 500° C, repeated melting occurs to produce pseudotachylyte. The high dislocation densities in the mylonites and extreme reduction in recrystallized grain size point to exceptionally high shear stresses during the ductile deformation. Interpretation of the mechanical response of the rock needs to encompass the absence of distinct brittle failure, the dominance of dislocation glide over climb in the host mylonite and the strong influence of grain size on defect substructures and, hence, flow mechanisms.

A principal difficulty resides in the identification of relevant flow laws for quantifiying the possible rheological behaviour. Hobbs *et al.* (1986) utilized flow data from Shelton & Tullis (1981) to analyze the development of plastic instabilites in the mid-crust. Both limitations of experimental apparatus (Gleason & Tullis 1993) and unconstrained effects of water fugacity (Kohlstedt *et al.* 1995) have been identified as sources of error in these flow laws. This is particularly inconvenient given that Shelton & Tullis (1981) contains the only flow laws for feldspar-rich rocks.

An attempt is made herein to reconcile some of these stated problems by recasting the relationships with a strength correction (Gleason & Tullis 1993) and introducing a water fugacity dependence for strain rate (Kohlstedt *et al.* 1995). To test the results, a comparison is made using a more current diabase flow law established under extremely anhydrous, thermodynamically buffered conditions (Mackwell *et al.* 1995) and the adjusted Shelton & Tullis (1981) diabase flow law. The Shelton & Tullis (1981) flow laws are reformulated by first calculating the strain rate they predict for 900° C and a stress difference of 450 MPa (i.e. typical experimental conditions). This strain rate is then used to re-calculate the stress exponent, n, assuming that the differential stress was half that quoted (i.e. 225 MPa) as suggested by Gleason & Tullis (1993). This produces $n=3.6$ for anorthosite and $n=3.8$ for diabase. Next, a linear dependence of strain rate on water fugacity (Kohlstedt *et al.* 1995) is assumed, with the Mackwell *et al.* (1995) data taken to reflect a base-line null effect, and the Shelton & Tullis (1981) flow laws normalized relative to the experimental confining pressure of 1.5 GPa (Kerrick & Jacobs 1981).

For conditions under which field evidence exists for ductile deformation of diabase (e.g. 700° C and 750 MPa based on temperature and pressure gradients of $dT/dz \approx 25°\,C\,km^{-1}$ and $dP/dz \approx 27\,MPa\,km^{-1}$), diabase flow laws from both of the latter sources give the same strain rate of $6 \times 10^{-12}\,s^{-1}$ for 100 MPa differential stress when the stated adjustments are made. These are clearly crude estimates that require a pure water phase, thermodynamic saturation of related point defects and a poorly constrained strength adjustment; nevertheless, they serve to emphasize the potential similarities between outwardly disparate flow laws, as elegantly demonstrated by Kohlstedt *et al.* (1995) for quartz.

When similarly recalculated for a temperature and confining pressure appropriate to Seaforth Head (e.g. 500° C and 550 MPa confining pressure), the adjusted Shelton & Tullis (1981) flow law for anorthosite gives $2 \times 10^{-14}\,s^{-1}$ at 100 MPa differential stress. The latter strain rate/stress quantities are consistent with the onset

of dislocation creep in the mid-crust at 450–500° C, suggesting that, although the details of the flow law may be in question, the gross rheological description may be appropriate

Paleostress estimates and crustal strength

The magnitude of stress during pseudotachylyte formation is critical to interpretation of plausible formation mechanisms. Paleopiezometry is hobbled by the general paucity of experimental data for realistic empirical piezometers. Nevertheless, recrystallized grain size and dislocation density have been examined in an attempt to extract information regarding paleostresses.

Dislocation density has been related to differential stress (Takeuchi & Argon 1976) through the relationship

$$\sigma_1 - \sigma_3 = \alpha G \mathbf{b} \rho^{1/2} \quad (1)$$

where α is a constant approximately equal to 3 (Briegel & Goetze 1978, Kohlstedt & Weathers 1980), G is the appropriate shear modulus, $\mathbf{b}$ is a representative Burgers vector and ρ is the dislocation density. Similarly, recrystallized grain diameter, d, has been related to stress (Takeuchi & Argon 1976, Poirier 1985) as

$$\sigma_1 - \sigma_3 = \beta G(\mathbf{b}/d)^c \quad (2)$$

where β and c are material constants. A variety of silicates have empirically-established c values ranging from 0.67–0.84 (Kohlstedt & Weathers 1980, Poirier 1985). For quartz, values of $c = 0.7$ $\beta = 3.8$, $\mathbf{b} = 0.5$ nm and $G = 44$ GPa were used (White 1982).

An empirical feldspar piezometer was constructed from experimental data (Tullis & Yund 1985, Tullis *et al.* 1990) for which the recrystallized grain size and microstructures corresponded to those observed in the Seaforth Head samples. Grain size–stress relationships were estimated at 10% and 25% axial strains and 500 nm (Tullis *et al.* 1990) at 410 MPa (10% strain) and 380 MPa (25% strain) and 1 μm (Tullis & Yund 1985) at 240 MPa (10% strain) and 220 MPa (25% strain). The quoted error in stress for these experiments is ± 50 MPa (Tullis & Yund 1985) using a NaCl solid medium apparatus which compares favourably with measurements in molten salt cells (Gleason & Tullis 1993). The complete piezometers are:

$$\text{at 10\% strain} \quad \sigma_1 - \sigma_3 = 1.7G(\mathbf{b}/d)^{0.77} \quad (3)$$

$$\text{and at 25\% strain} \quad \sigma_1 - \sigma_3 = 1.6G(\mathbf{b}/d)^{0.78} \quad (4)$$

Stresses calculated using both piezometers are consistent with stress levels expected in the crust for a variety of recrystallized grain sizes. Mean values of $\mathbf{b} = 0.78$ nm and $G = 35$ GPa (Gandais & Willaime 1984) were used for both plagioclase and K-feldspar.

The range of stresses determined by the various piezometers is shown in Fig. 7. The estimated stresses exhibit a distinct lower cutoff at about 140 MPa. There is a strong overlap of the stress ranges calculated using either dislocation density or recrystallized grain size and

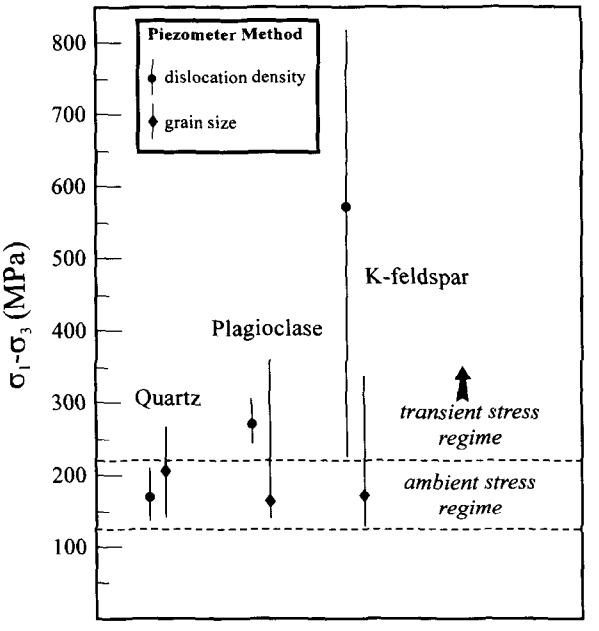

Fig. 7. Differential stress (σ_1–σ_3) estimates using different minerals. Feldpsar grain-size relationships are calculated from Equation (4) which gives lower estimates. The range of stresses that were calculated is given by the vertical line, with the average indicated by the symbol. There is a distinct lower cutoff at about 140 MPa in estimates for all methods. The concentration of means is used to infer an ambient stress regime on which are imposed higher transient stresses.

means of calculated stresses are typically skewed toward the lower end of the range (<210 MPa) for a given piezometer. The stress ranges are interpreted to reflect a preserved record of ambient shear zone stresses of the order 140–210 MPa, with the heterogeneous development of larger transient stresses. Interpretation of the high dislocation-density-related stresses as a simple overprint is rejected in light of the consistency of host-recrystallized grain microstructures and the related absence of dislocations cutting across both porphyroclasts and recrystallized grains.

Differential stress estimates from the mylonitic gneiss are typical of the 100–200 MPa values found in other mylonites (Briegel & Goetze 1978, Weathers *et al.* 1979, White 1979, Christie & Ord 1980, Kohlstedt & Weathers 1980, Hacker *et al.* 1990), albeit near the high end of the range. The apparent large deviation of paleostresses in excess of 200 MPa, in conjunction with the intense non-uniform flow, lends credence to arguments for intense stress and strain-rate transients during the shear zone deformation.

The development of crustal stresses in excess of 100 MPa, in general, requires low pore-fluid pressures; a 'normal' fluid-rich environment effectively limits brittle–ductile transitions to low-stress phenomena (Fig. 8). The transition from ductile to brittle behaviour of thrusted lower crustal material is thus controlled by access to free-fluid, in addition to temperature and pressure constraints on deformation mechanisms. What then is the effect of a water deficit on crustal deformation? The propensity for fluid flow in fault zones typically makes this question irrelevant. However, despite lithostatic fluid pressures in the deep crust, a low volume of free fluid in low-

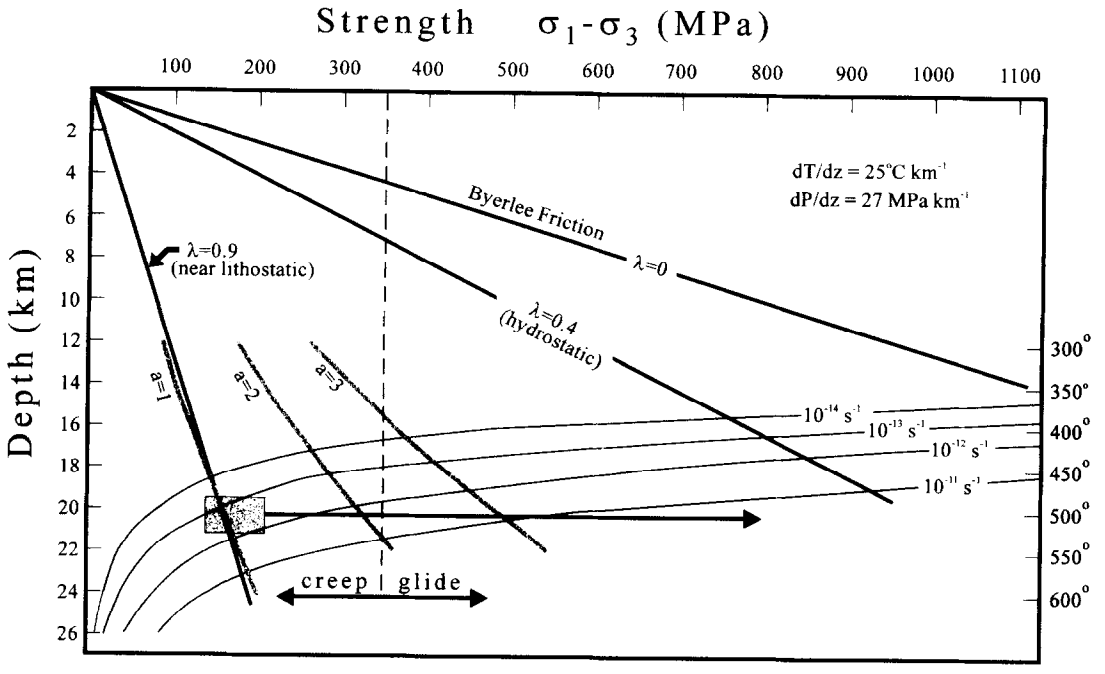

Fig. 8. Crustal strength diagram demonstrating the conditions under which plastic instabilities could develop in a thrust regime. Frictional strengths are calculated for an optimally oriented, reactivated thrust (Sibson 1990). λ = pore fluid pressure/lithostatic pressure. Ductile strengths are calculated from the modified Shelton & Tullis (1981) anorthosite rheology (see text). Ambient stresses are defined by the stippled box and centered on a temperature of 510° C. These stresses correlate to strain rates in the order of 10^{-13} s^{-1}. The complete range of estimated stresses is indicated by the thick horizontal arrow emanating from the box. The stress–temperature conditions under which plastic instabilities could develop are calculated for work hardening factors of $a = 1,2,3$ and are contoured respectively for depth–stress space that encompasses the conditions appropriate to this study. Significantly, the contour for $a = 1$ intersects the ambient stress range indicating that a work hardening factor of this magnitude could lead to instabilities without invoking high stresses. However, sufficiently high stresses have been inferred to accommodate $a = 3$.

permeability metamorphic rocks inhibits maintenance of distributed fluid pressures in any new fractures. A fluid-deficient environment potentially allows larger stresses to develop during thrust exhumation of deep crust. The ability to maintain these stresses is linked to accommodation of the deformation within the strongly temperature-sensitive, high-strength portion of the ductile strength curve (Fig. 8), at the expense of still higher-strength dry, brittle behaviour.

Deformation mechanisms

Deformation at Seaforth Head is a cyclic competition between regimes of strain and/or strain-rate hardening and softening, producing the extreme heterogeneity of microstructures and highly variable, non-uniform flow. Ultra-fine-grained material is produced by both melting and dynamic recrystallization. The bimodal defect microstructure defined by crystallographic and shape fabrics in the presence of high dislocation densities in the host mylonite and porphyroclasts, and equant grain shapes and negligible dislocation densities in fine-grained material is consistent with the activity of grain-size-sensitive (GSS) flow mechanisms, as have been invoked previously (Passchier 1982, Hobbs *et al.* 1986), to explain the apparent macroscopic superplasticity exhibited by deformed pseudotachylyte, i.e. large macroscopic strains with minimal evidence for intracrystalline deformation. The occurrence of dislocated and recrystallized porphyroclasts within dislocation-free ultramylonite grains indicates that GSS and dislocation creep mechanisms can be synchronous. Likewise, the synkinematic growth of pseudotachylyte grains toward an equilibrium grain size produced by dynamic recrystallization, comparable to that observed in naturally-deformed quartz of differing grain sizes, e.g. chert and quartzite (White 1982), suggests the mutual activity of crystal–plastic and GSS processes.

The validity and effects of invoking GSS flow have been examined through constitutive flow laws. A feldspar-rich material is assumed to be reasonably described in the dislocation creep field by the fugacity/strength adjusted anorthosite flow law of Shelton & Tullis (1981), where

$$\dot{\varepsilon} = A\exp(-Q_v/RT)\sigma^n \quad (5)$$

Grain-boundary sliding accommodated by dislocations in the grain mantle (Gifkins 1976) is assumed to be representative of GSS mechanisms, where

$$\dot{\varepsilon} = (64G\mathbf{b}/kT)D_o\exp(-Q_b/RT)(\mathbf{b}/d)^2(\sigma/G)^2 \quad (6)$$

[$\dot{\varepsilon}$, strain rate; A, experimentally-derived coefficent; Q_v, activation energy for dislocation creep associated with intracrystalline diffusion; R, gas constant; T, deformation temperature in Kelvin; σ, differential stress; n, experimentally-determined stress exponent; k, Boltzmann's constant; D_o, pre-exponential coefficient for diffusion; Q_b, activation energy for grain-boundary-diffusion-controlled creep].

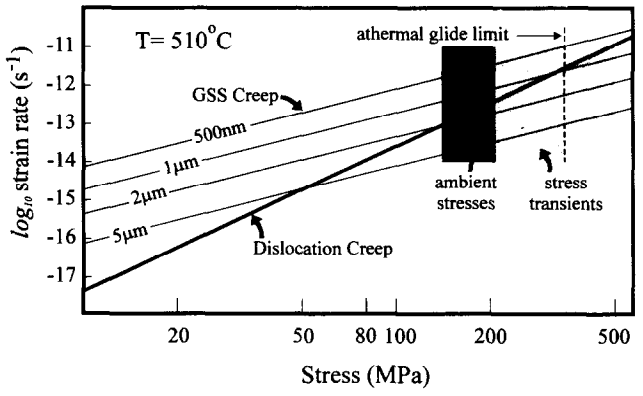

Fig. 9. Strain rate vs differential stress plot for dislocation creep (heavy line) and dislocation-accommodated grain-boundary sliding for grain sizes of 0.5, 1, 2 and 5 μm. From this plot, the regimes in which a given mechanism will dominate (i.e. a faster strain rate for fixed stress, or lower stress from fixed strain rate) can be inferred. Of note is the apparent ability of very-fine-grained material to accommodate flow by a grain-size-sensitive mechanism even at relatively high stress levels. Once formed, the ultramylonite (deformed pseudotachylyte) is capable of maintaining ambient strain rates at lower stress levels than that at which the melt formed.

Equation (6) is chosen in recognition of the microstructural evidence for combined GSS and dislocation flow. The invocation of other GSS flow mechanisms such as Coble creep or Ashby-Verall sliding would only enhance the grain-size sensitivity. Dislocation creep and GSS flow are then assumed to contribute equally to the strain rate at an equilibrium grain size of approximately 2 μm, $T = 510°$ C and a strain rate of $1 \times 10^{-13}\ s^{-1}$ as described by Equation (5) Fig. 9. The activation energy, Q_b is set at 2/3 Q (Frost & Ashby 1982), allowing calculation of D_o for use in Equation (6).

The overall effect of GSS flow will be development of strain-rate heterogeneities $\partial\dot{\gamma}/\partial\gamma > 0$ for constant stress, or large stress reductions, $\partial\tau/\partial\gamma < 0$ for constant strain rate, where $\dot{\gamma}$ is shear-strain rate, γ is shear strain and τ is shear stress. For example, pseudotachylyte introduced into an ambient stress level of 140 MPa could maintain strain rates of 1×10^{-11} and $4 \times 10^{-13}\ s^{-1}$ for grain sizes of 200 nm and 1 μm, respectively, compared to $1 \times 10^{-13}\ s^{-1}$ for the deforming host. The introduction of fine-grained, polymineralic pseudotachylyte with self-pinning grain boundaries would have the additional effect of stabilizing grain sizes below that prescribed by the equilibrium recrystallized grain size. The fine-grained pseudotachylyte could, without microstructural re-equilibration, maintain stresses up to that corresponding to the equivalent recrystallized grain size, suppressing the need to develop low-stress defect substructures and explaining the apparent abrupt cut-off in observed stresses.

Dislocation glide dominates the defect microstructure of coarse-grained material, in contrast to the more typical recovery substructures associated with dislocation creep, and as observed in experimentally-deformed feldspars (Tullis & Yund 1985). This exceptional dislocation activity and absence of subgrains reflects the dominance of glide over climb, consistent with deformation in a high-stress, glide-dominated regime. The creep/athermal glide boundary for many materials is estimated at $10^{-2}\ G$ (Frost & Ashby 1982) or 350 MPa for feldspar. This value falls within the most accessible region of the inferred transient stress regime (Fig. 7), consistent with excursions into the higher stress, glide-dominated field that generates the high dislocation densities.

Plastic instabilities and pseudotachylyte regimes

Hobbs *et al.* (1986) developed a criterion for identifying conditions under which plastic instabilities can occur wherein the critical work hardening condition, $\partial\tau/\partial\gamma$, is

$$\partial\tau/\partial\gamma < (\tau Q/nRT^2)\cdot(\kappa\tau/c\rho) \qquad (7)$$

[Q, activation energy for the appropriate creep mechanism; c is specific heat; ρ, density of deforming rock; κ, fraction of heat retained in the system where $\kappa = 1$, for adiabatic case].

Alternatively, $\partial\tau/\partial\gamma$ can be re-written as a fraction of the operative shear stress for an incremental strain, $a\tau$, where a is defined as the work hardening factor. The critical temperature below which instabilities can develop for a fixed stress/strain rate is then

$$T_c > (Q/anR)\cdot(\kappa\tau/c\rho)^{1/2}. \qquad (8)$$

In their discussion of continental shear zones, Hobbs *et al.* (1986) utilized a value of $a = 66.6$, while indicating that smaller values of a will raise T_c. The ratio of maximum to inferred ambient stresses at Seaforth Head (Table 1) suggests that a most likely lies between 2 and 3, with a maximum value of 6. Hobbs & Ord (1988) have argued subsequently in discussion of subduction-related instabilities that a is of the order 1, in closer correspondence with the Seaforth Head estimates.

The test of whether the pseudotachylyte at Seaforth Head can be related to instability theory rests on determining if the deformation temperature falls in the field delimited by Equation (8) and, in turn, if the related stress needed to initiate instability at that temperature corresponds to a reasonable strain rate through some flow law.

The stress–temperature space in which instabilities can develop for $a = 1$, 2 and 3 has been calculated using the adjusted anorthosite flow law of Shelton & Tullis (1981). The minerals are assumed to be water-saturated based on the presence of hydrous phases, but with minimal free-fluid. These fields are plotted in Fig. 8 and clearly demonstrate the feasibility of instability formation under the conditions established for Seaforth Head.

For ambient conditions of $T = 510°C$, $\sigma_1 - \sigma_3 = 210$ MPa and $\dot{\varepsilon} \approx 4 \times 10^{-13}\ s^{-1}$, instability formation requires differential stresses in the order of 300 MPa and 450 MPa for work hardening factors $a = 2$ and 3, respectively, well within the range of observed paleostresses. The required deviation from inferred ambient conditions requires strain rate perturbations of less than an order of magnitude (e.g. $4 \times 10^{-13} \rightarrow 10^{-12}\ s^{-1}$).

Notably, instabilities are predicted only in the 'flat' portion of the ductile strength curve at stresses that

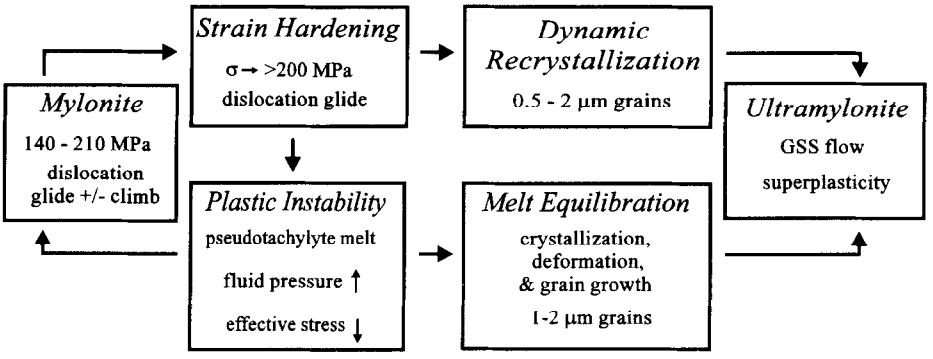

Fig. 10. Summary diagram of microstructure and mechanism paths during mylonite–pseudotachylyte–ultramylonite formation.

correspond to the anticipated onset of athermal glide. Because many, if not most, natural deformation studies involve situations with significant pore-fluid activity that preclude development of high strength ductility, evidence for this portion of the strength curve may, in practice, be rarely accessed. The ambient stress (≈140–210 MPa) remains at the upper end of those characteristic of mylonite zones, consistent with an undersaturated fluid environment, and at the lower limit for which plastic instabilities are predicted. This creates a situation whereby a background 'normal' shear zone develops at unexceptional strain rates (10^{-12}–10^{-13} s^{-1}), but for which only moderate stress/strain-rate perturbations are needed to cycle material into the regime of instability formation. Runaway instabilities could then generate the temperature transients needed for pseudotachylyte formation (Hobbs *et al.* 1986).

The small magnitude of the required strain-rate perturbations is consistent with the apparent frequency with which the pseudotachylyte-forming events occur, and the ensuing large total volume fraction of pseudotachylyte in the shear zone. Additionally, the development of thermo-mechanical instability may be contingent upon activating massive dislocation glide. This largely follows from the restriction of instability fields to the high-strength ductile regime where glide will necessarily dominate. The general preclusion of seismicity in the deep crust may not be justified, nor require extraordinary high differential stresses or high fluid pressures. Identification of similar high stress and strain-rate ductility at granulite conditions (White & Jiang 1994) poses the possibility that low-fluid pressure conditions and the ensuing-high strength ductile flow of rock are intimately linked to instabilities that might lead to seismic events and melting. The deformation history is summarized in Fig. 10.

CONCLUSIONS

(A) Pseudotachylyte is produced cyclically as a melt during mylonitization within the Outer Hebrides thrust. The pseudotachylyte is synkinematic with the mylonite and ambient deformation conditions lie well within the ductile field at temperatures in the order of 500° C

(B) Paleostress estimates infer deformation at relatively high differential stresses (140–210 MPa) giving unexceptional strain rates (10^{-13} s^{-1}), on which are imposed transient high stresses reflecting the inherently heterogenous nature of flow.

(C) The inferred stress levels, when combined with experimental flow laws and the temperature estimate are sufficient to generate plastic instabilities during ductile flow, without invoking frictional slip, for which there is no evidence.

(D) Low pore-fluid pressure is a requirement for generation of plastic instabilities in that high-strength ductile flow is achieved only in the absence of low effective-stress brittle processes. The extensive dislocation glide associated with high-strength ductile flow may be a necessary precursor to the instability.

(E) Ultramylonites in such systems can be produced along two paths. One comprises dislocation processes leading to grain size reduction by dynamic recrystallization, while the other involves deformation of fine-grained crystallized melt. Grain size reduction by both processes enhances grain-size-sensitive flow and contributes to the overall non-uniform flow within these rocks.

Acknowledgements—Formulation of this work has been influenced over many years by several colleagues, to whom thanks are due: J. Starkey initially whetted an interest in pseudotachylyte, I. Allison has provided field logistics and scientific companionship over a long period and R. H. Sibson generously provided his original study material. Instrumental facilities and technical support were provided by the UNB Electron Microscopy Unit. Reviews by G. Hirth and L. Dell'Angelo were helpful in clarifying several issues. This study was supported by NSERC Research Grant A8512.

REFERENCES

Austrheim, H. & Boundy, T. M. 1994. Pseudotachylytes generated during seismic faulting and eclogization of the deep crust. *Science* **265**, 82–83.

Brace, W. F. & Kohlstedt, D. L. 1980. Limits on lithospheric stress imposed by laboratory experiments. *J. geophys. Res.* **85**, 6248–6252.

Briegel, U. & Goetze, C. 1978. Estimates of differential stress recorded in the dislocation substructure of Lochseiten limestone (Switzerland). *Tectonophysics* **48**, 61–76.

Brown, W. & Parsons, I. 1989. Alkali feldspars: ordering rates, phase

transformations and behaviour diagrams for igneous rocks. *Mineral. Mag.* **53**, 25–42.
Brun, J. P. & Cobbold, P. 1980. Strain heating and thermal softening in continental shear zones: a review. *J. Struct. Geol.* **2**, 149–158.
Byerlee, J. D. 1978. Friction of rocks. *Pure appl. Geophys.* **116**, 615–626.
Christie, J. M. & Ord, A. 1980. Flow stress from microstructures of mylonites: example and current assessment. *J. geophys. Res.* **85**, 6253–6262.
Clarke, G. L. & Norman, A. R. 1993. Generation of pseudotachylyte under granulite facies conditions, and preservation during cooling. *J. metam. Geol.* **11**, 319–335.
Cumbest, R. J., Drury, M. R., van Roermund, H. L. M. & Simpson, C. 1989. Dynamic recrystallization and chemical evolution of clinoamphibole from Senja, Norway. *Contrib. Miner. Petrol.* **101**, 339–349.
Eggleton, R. A. & Buseck, P. R. 1980. The orthoclase–microcline inversion: a high-resolution TEM study and strain analysis. *Contrib. Miner. Petrol.* **74**, 123–133.
Engelder, T. 1993. *Stress Regimes in the Lithosphere.* Princeton University Press.
Etheridge, M. A. 1983. Differential stress magnitudes during regional deformation and metamorphism: Upper bound imposed by tensile fracturing. *Geology* **11**, 231–234.
Fleitout, L. & Froidvaux, C. 1980. Thermal and mechanical evolution of shear zones. *J. Struct. Geol.* **2**, 159–164.
Francis, P. W. & Sibson, R. H. 1973. The Outer Hebrides Thrust. In: *The Early Precambrian of Scotland and Related Rocks of Greenland* (edited by Park, R. G. & Tarney, J.). University of Keele.
Frischbutter, A. & Hanisch, M. 1991. A model of granitic melt formation by frictional heating on shear planes. *Tectonophysics* **194**, 1–11.
Frost, H. J. & Ashby, M. F. 1982. *Deformation-Mechanism Maps: The Plasticity and Creep of Metals and Ceramics.* Pergamon Press, Oxford.
Gandais, M. & Willaime, C. 1984. Mechanical properties of feldspars. In: *Feldspars and Feldspathoids* (edited by Brown, W. L.). Riedel.
Gifkins, R. C. 1976. Grain boundary sliding and its accommodation during creep and superplasticity. *Metal. Trans.* **7A**, 1225–1232.
Gleason, G. C. & Tullis, J. 1993. Improving flow laws and piezometers for quartz and feldspar aggregates. *Geophys. Res. Lett.* **20**, 2111–2114.
Hacker, B. R., Yin, A., Christie, J. M. & Snoke, A. W. 1990. Differential stress, strain rate and temperatures of mylonitization in the Ruby Mountains, Nevada: implications for the rate and duration of uplift. *J. geophys. Res.* **95**, 8569–8580.
Hanks, T. C. 1977. Earthquake stress drops, ambient tectonic stresses, and the stresses that drive plate motions. *Pure appl. Geophys.* **115**, 441–458.
Hanks, T. C. & Raleigh, C. B. 1980. The conference on magnitude of deviatoric stresses in the Earth's crust and upper mantle. *J. geophys. Res.* **85**, 6083–6085.
Hobbs, B. E. & Ord, A. 1988. Plastic instabilities: implications for the origin of intermediate and deep focus earthquakes. *J. geophys. Res.* **93**, 10521–10540.
Hobbs, B. E., Ord, A. & Teyssier, C. 1986. Earthquakes in the ductile regime. *Pure appl. Geophys.* **124**, 309–336.
Kerrick, D. M. & Jacobs, G. K. 1981. A modified Redlich–Kwong equation for H_2O, CO_2, and H_2O–CO_2 mixtures at elevated pressures and temperatures. *Am. J. Sci.* **281**, 735–767.
Koch, N. & Masch, L. 1992. Formation of Alpine mylonites and pseudotachylytes at the base of the Silvretta nappe, Eastern Alps. *Tectonophysics* **204**, 289–306.
Kohlstedt, D. L. & Weathers, M. S. 1980. Deformation-induced microstructures, paleopiezometers, and differential stresses in deeply eroded fault zones. *J. geophys. Res.* **85**, 6269–6285.
Kohlstedt, D. L., Evans, B. & Mackwell, S. J. 1995. Strength of the lithosphere: Constraints imposed by laboratory experiments. *J. geophys. Res.* **100**, 17587–17602.
Mackwell, S. J., Zimmerman, M. E., Kohlstedt, D. L. & Scherber, D. S. 1995. Experimental deformation of dry Columbia Diabase: implications for tectonics on Venus. *U.S. Symp. Rock Mech.* **35**, 207–214.
McKenzie, D. & Brune, J. N. 1972. Melting on fault planes during large earthquakes. *Geophys. J. R. ast. Soc.* **29**, 65–78.
Mercier, J.-C. C. 1980. Magnitude of the continental lithospheric stresses inferred form rheomorphic petrology. *J. geophys. Res.* **85**, 6293–6303.
Nicolas, A., Bouchez, J. L., Blaise, J. & Poirier, J. P. 1977. Geological aspects of deformation in continental shear zones. *Tectonophysics* **42**, 55–73.
Nyman, M. W., Law, R. D. & Smelik, E. A. 1992. Cataclastic deformation mechanism for the development of core–mantle structures in amphibole. *Geology* **20**, 455–458.
Ord, A. & Hobbs, B. E. 1989. The strength of the continental crust, detachment zones and the development of plastic instabilities. *Tectonophysics* **158**, 269–289.
Passchier, C. W. 1982. Pseudotachylyte and the development of ultramylonite bands in the Saint-Barthélemy Massif, French Pyrenees. *J. Struct. Geol.* **4**, 69–79.
Pavlis, T. L. 1986. The role of strain heating in the evolution of megathrusts. *J. geophys. Res.* **91**, 12407–12422.
Poirier, J.-P. 1985. *Creep of Crystals: High-temperature Deformation Processes in Metals, Ceramics and Minerals.* Cambridge University Press.
Pryer, L. L. 1993. Microstructures in feldspars from a major crustal thrust zone: the Grenville Front, Ontario, Canada. *J. Struct. Geol.* **15**, 21–36.
Robinson, P., Spear F. S., Schumaker, J. C., Laird, J., Klein, C. & Evans, B. W. 1982. Phase relations of metamorphic amphiboles: natural occurrence and theory. In: *Amphiboles: Petrology and Experimental Phase Relations* (edited by Veblen, D. R. & Ribbe, P. H.). *Mineral. Soc. Am. Rev. Mineral.* **9B**, 1–122.
Scholz, C. H. 1980. Shear heating and the state of stress on faults. *J. geophys. Res.* **85**, 6174–6184.
Scholz, C. H. 1990. *The Mechanics of Earthquakes and Faulting.* Cambridge University Press.
Shelton, G. & Tullis, J. 1981. Experimental flow laws for crustal rocks. *EOS Trans. Am. Geophys. Un.* **62**, 396.
Shimamoto, T. 1985. The origin of large or great thrust-type earthquakes along subducting plate boundaries. *Tectonophysics* **119**, 37–65.
Sibson, R. H. 1974. Frictional constraints on thrust, wrench and normal faults. *Nature* **249**, 542.
Sibson, R. H. 1975. Generation of pseudotachylyte by ancient seismic faulting. *Geophys. J. R. ast. Soc.* **43**, 775–794.
Sibson, R. H. 1977. Fault rocks and fault mechanisms. *J. geol. Soc. Lond.* **133**, 192–214.
Sibson, R. H. 1980a. Transient discontinuities in ductile shear zones. *J. Struct. Geol.* **2**, 165–174.
Sibson, R. H. 1980b. Power dissipation and stress levels on faults in the upper crust. *J. geophys. Res.* **85**, 6239–6247.
Sibson, R. H. 1984. Roughness at the base of the seismogenic zone: contributing factors. *J. geophys. Res.* **89**, 5791–5799.
Sibson, R. H. 1986. Earthquakes and rock deformation in crustal fault zones. *Ann. Rev. Earth Planet. Sci.* **14**, 149–175.
Sibson, R. H. 1990. Faulting and fluid flow. In: *Fluids in Tectonically Active Regimes of the Continental Crust* (edited by Nesbitt, B. E.). *Mineral. Assoc. Can. Short Course* **18**, 93–132.
Spear, F. S. 1980. NaAl⇌CaAl exchange equilibrium between plagioclase and amphibole. *Contrib. Miner. Petrol.* **72**, 33–41.
Spray, J. G. 1987. Artificial generation of pseudotachylyte using friction welding apparatus: Simulation of melting on a fault plane. *J. Struct. Geol.* **9**, 49–60.
Stesky, R. M. 1978. Mechanisms of high temperature frictional sliding in Westerly granite. *Can. J. Earth. Sci.* **15**, 361–375.
Stesky, R. M., Brace, W. F., Riley, D. K. & Robin, P.-Y. F. 1974. Friction in faulted rock at high temperature and pressure. *Tectonophysics* **23**, 177–203.
Takeuchi, S. & Argon, A. S. 1976. Steady-state creep of single phase crystalline material at high temperatures. *J. Mat. Sci.* **11**, 1542–1566.
Tullis, J. & Yund, R. A. 1985. Dynamic recrystallization of feldspar: a mechanism for ductile shear zone formation. *Geology* **14**, 238–241.
Tullis, J. & Yund, R. A. 1987. Transition from cataclastic flow to dislocation creep of feldspar: Mechanisms and microstructures. *Geology* **15**, 606–609.
Tullis, J. & Yund, R. A. 1992. The brittle–ductile transition in feldspar aggregates: An experimental study. In: *Fault Mechanics and Transport Properties of Rocks* (edited by Evans, B. & Wong, T.-F.). Academic Press, New York, 89–117.
Tullis, J., Dell'Angelo, L. N. & Yund, R. A. 1990. Ductile shear zones from brittle precursors in feldspathic rocks. In: *The Brittle–Ductile Transition in Rocks* (edited by Duba, A. G., Durham, W. B., Handin, J. W. & Wang, H. F.). Geophys. Mono. **56**. Am. Geophys. Un., Washington, D. C., 67–81.
Turner, F. J. 1968. *Metamorphic Petrology.* McGraw-Hill, New York.
Weathers, M. S., Bird, J. M., Cooper, R. F. & Kohlstedt, D. L. 1979. Differential stress determined from deformation-induced microstructures of the Moine thrust zone. *J. geophys. Res.* **84**, 7495–7509.
White, S. 1979. Paleo-stress estimates in the Moine Thrust zone, Eriboll, Scotland. *Nature* **280**, 222–223.

White, J. C. 1982. Quartz deformation and the recognition of recrystallization regimes in the Flinton Group conglomerates, Ontario. *Can. J. Earth Sci.* **19**, 1982.
White, J. C. & Jiang, D. 1994. High-strength ductile behaviour of ancient lower continental crust: evidence from natural deformation. *EOS Trans. Am. Geophys. Un.* **75**, 329.
White, J. C. & White, S. H. 1983. Semi-brittle deformation within the Alpine fault zone, New Zealand. *J. Struct. Geol.* **5**, 579–589.